Thermochimica Acta 471 (2008) 90–96

Contents lists available at ScienceDirect

Thermochimica Acta

journal homepage: www.elsevier.com/locate/tca

Modulated calorimetry of poly(1,4-oxybenzoate), poly(2,6-oxynaphthoate), and their copolymers☆

J. Ma[a,b], A. Habenschuss[b], B. Wunderlich[a,b,*]

[a] Department of Chemistry, University of Tennessee, Knoxville, TN 37996-1600, USA
[b] Chemical Sciences Division, Oak Ridge National Laboratory, Oak Ridge, TN 37831-6197, USA

ARTICLE INFO

Article history:
Received 20 January 2008
Received in revised form 23 February 2008
Accepted 9 March 2008
Available online 18 March 2008

Keywords:
Poly(1,4-oxybenzoate)
Poly(2,6-oxynaphthoate)
Copolymer
Reversing transition
Temperature-modulated DSC
Condis crystal

ABSTRACT

Poly(1,4-oxybenzoate) (POB) and poly(2,6-oxynaphthoate) (PON) and their copolymers which have a well-established phase diagram have been studied with temperature-modulated differential scanning calorimetry (TMDSC). All the analyzed polymers have more than one disordering transition between the glass transition (from 400 to 430 K) and decomposition (starting at ≈700 K). Above the glass transition, the reversible heat capacity, C_p, increases beyond that calculated from the crystallinity and the known C_p of the solid and melt. This is likely due to an increase of mobility within the crystals and/or a possible rigid-amorphous fraction (mainly for the copolymers). The disordering transitions are largely irreversible, supporting the observation that semicrystalline, linear macromolecules show decreasing amounts of locally reversible melting with increasing rigidity and crystal perfection.

Published by Elsevier B.V.

1. Introduction

The three-dimensional structures of poly(4-oxybenzoate) (POB) and poly(2,6-oxynaphthoate) (PON) have been of particular interest, owing to their physical properties and industrial applications [1–4]. Copolymers of the monomers *p*-hydroxybenzoic acid (HBA) and 2,6-hydroxynaphthoic acid (HNA) have been produced with the aim of improving moldability and processability [5]. The chemical structures of the repeating units of POB and PON are given by

POB PON

In the earlier studies of the homopolymers and copolymers by differential scanning calorimetry (DSC), two or more phase transitions were observed before isotropization or thermal decomposition [6–13]. The phase diagram of the largely metastable system was established recently and is redrawn in Fig. 1 [14]. It is based mainly on zero-entropy-production transition temperatures, measured on heating. The reversing and reversible nature of the transitions is investigated in the present research on the samples marked on the upper abscissa.

For POB, the lowest endothermic transitions occur, depending on thermal history, between 616 and 633 K (T_1) with a large entropy of disordering (9.3 J/(K mol) [14]). This transition is a change from the orthorhombic, rigid crystals to a conformationally disordered pseudo-hexagonal phase (condis phase) [11,12]. Conformationally disordered (condis) crystals show large-amplitude, internal-rotational mobility [15]. Based on this molecular motion, the condis crystals have also been called one-dimensional plastic crystals or ordered smectic phases. On cooling without an ordering transition, a (plastic) condis crystal freezes into a solid condis glass [15], a most important transition, because it limits most of the applications to lower temperature and above, it permits the deformations needed to shape the objects made of the polymers. The next transition of POB in Fig. 1, at 718 K (T_2), involves a small, broad endotherm with an entropy of transition of only 0.5 J/(K mol). It is caused by an additional disordering process, involving no change in the packing and order along the chain axis or chain conformation, but a loss of long-range phenyl orientation in the *a*–*b* plane. A further change to an anisotropic melt (liquid crystal) occurs at ≈800 K (T_3) with increasing decomposition above 750 K. An indication of

☆ This manuscript has been authored by a contractor of the U.S. Government under the contract no. DOE-AC05-00OR22725. Accordingly, the U.S. Government retains a non-exclusive, royalty-free license to publish or reproduce the published form of this contribution, or allow others to do so, for U.S. Government purposes.

* Corresponding author at: Department of Chemistry, University of Tennessee, Knoxville, TN 37996-1600, USA. Tel.: +1 865 675 4532.
E-mail address: Wunderlich@CharterTN.net (B. Wunderlich).

0040-6031/$ – see front matter. Published by Elsevier B.V.
doi:10.1016/j.tca.2008.03.004

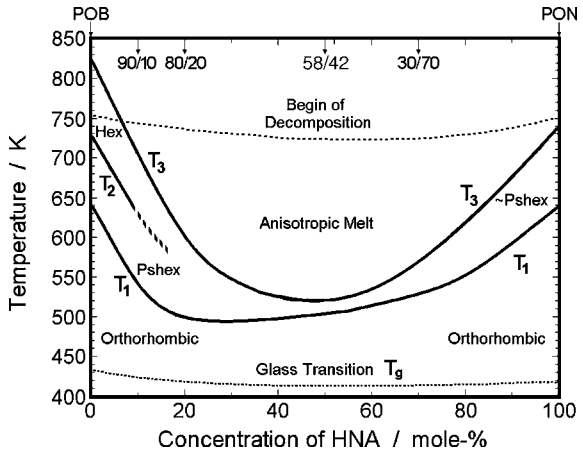

Fig. 1. A phase diagram of POB, PON and their copolymers as derived from heating experiments. Derived from DSC, thermogravimetry, and X-ray diffraction [14]. The lines labeled T_1, T_2, and T_3 refer to transitions with latent heats.

the ultimate melting (isotropization) of single crystals of POB, and also of PON, was reported above 800 K [16,17], but is accompanied by considerable decomposition.

Much less information is available about the structure of PON. Prior calorimetry in our laboratory has shown broad transitions between 610 and 710 K (T_1) [8,9]. The transition T_1 also involves a change from orthorhombic to nearly pseudo-hexagonal, which changes at T_3 to a phase with considerable rotational freedom of the naphthalene units [14]. The transition T_3 became evident from the work of Mühlebach et al., using DSC, thermomechanical analysis (TMA), and electron and optical microscopy by extending the measurements into the decomposition region [13]. This second transition leads to a more mobile mesophase that has been proposed to be a nematic liquid crystal (anisotropic melt). In addition to DSC, infrared spectroscopy (IR), optical microscopy, and X-ray studies were carried out on whiskers of PON beyond the second transition [17]. A large endotherm was seen above 800 K, which is in the decomposition region, and may involve the final randomization of the chains.

The thermal properties of the copolymers have been studied in considerable detail up to 650 K (somewhat below decomposition), including heat capacity, C_p, enthalpy, entropy and Gibbs function, and the transition behavior [8,9]. The glass transition temperatures of the copolymers are located at 405–430 K (T_g), but the transition ranges are rather broad (from 160–200 K in width). Their ΔC_p changes little with composition (35–42 J/(K mol)) [9]. The C_p for the crystal, glass, and anisotropic melt is additive relative to the homopolymers. The crystallization of the 75, 58, and 30 mol% HBA copolymers to the pseudo-hexagonal phase was shown to be fast, and is followed by slow annealing to the orthorhombic crystals at sufficiently low temperatures [7,9]. The kinetics was reported based on calorimetry [10] and X-ray analysis [18].

The X-ray diffraction data of the copolymers reveal a high-axial orientation and three-dimensional order, while the meridional reflections are aperiodic. The molecular structure of the copolyesters is rather interesting. Biswas and Blackwell [19–21] proposed that the structure of the copolymer with a 75/25 composition of HBA/HNA consists of arrays of parallel chains of the random copolymer sequence in a *para*-crystalline structure [5]. In their model, the definition of the chain register is obtained by monomers on each chain being in the same horizontal plane, i.e., the repeat distance along the fiber axis is equal to the average dimer length. A different model of a non-periodic layer structure was proposed by Windle and co-workers [22–24]. In this model, the matching is calculated for short sequences of identical chemical structure from their random occurrence in parallel chains. Such a model was earlier used for a computer evaluation of accidental matches on cold crystallization of copolymers of poly(ethylene terephthalate-*co* sebacate) [25]. A more detailed comparison of the two HBA/HNA copolymer models is given in Ref. [26]. The crystal structure above the disordering transition was suggested to be a condis crystal with rotational disorder. This is also supported by evidence from mechanical and dielectric relaxation measurements [12,27,28].

In the present paper the past work [14] is extended by a study of the reversibility of the transitions. All the analyzed transitions indicate some reversing and very little reversible behavior, as one would expect for stiff condis crystals. Note that we designate the C_p as obtained by temperature-modulated DSC (TMDSC) as reversing. It refers to data which may still contain contributions from slowly decaying irreversible processes. Only if by extended, quasi-isothermal experiments a constant response is obtained, is the term reversible used. Note that the apparent, measured reversing $C_p^{\#}(\mathrm{exp})$ is equal to the absolute value of the measured complex heat capacity: $|C_p| = (C'^2_p + C''^2_p)^{1/2}$, with C'_p representing the real part ($=|C_p|\cos\theta$) and C''_p representing the imaginary (dissipative) part ($=|C_p|\sin\theta$) with θ representing the phase shift.

2. Experimental

2.1. Materials

The polymers used in this study were composed of HBA and HNA in the mole ratios of 100/0, 90/10, 80/20, 58/42, 30/70, and 0/100 (the HBA component is listed first). The copolymers and PON were commercial samples, prepared as described in Ref. [29] and used without any further treatment. They were provided many years ago in the form of pellets by the Hoechst-Celanese Research Co. All samples correspond to the ones used earlier [8,9,14]. The analyses of POB were done on single crystals, supplied by Dr. Kricheldorf of the University of Hamburg. Their synthesis from highly purified acetoxybenzoic acid is described in Refs. [30,31] (and correspond to the samples, marked as B in Ref. [14]).

2.2. Differential scanning calorimetry

A power-compensated PerkinElmer DSC-7® with a two-stage intra-cooler and a Pyris-1® system with liquid nitrogen cooling were employed for the calorimetry. The data are collected on a PC with the Pyris V7.0® software. Purified nitrogen gas was used as purge gas. During the measurements, the dry nitrogen gas was allowed to flow through the DSC cell at a rate of 20 mL/min. The temperature calibration was done with indium, tin, lead and zinc with masses of 4–6 mg. The heat of fusion was calibrated with indium, tin, and lead with masses of 6–10 mg. A standard sapphire disc served as reference for the C_p calibration, done at every temperature of interest. The standard heating rate was 10 K/min. Before calibrations, the baseline curvature of the empty cell was adjusted to make the deviations of the baseline less than 0.2 mW in the temperature range of interest between 300 and 650 K. This was followed by adjusting the initial and final isotherms to within 0.2 mW. The reversing and total heat capacities of the temperature-modulated DSC were calculated with the Pyris software.

The commonly used sawtooth modulation yields the reversing C_p from the first harmonic of the Fourier transformation of the heat-flow rate response. The total C_p is then the sliding average over one modulation cycle [32–34].

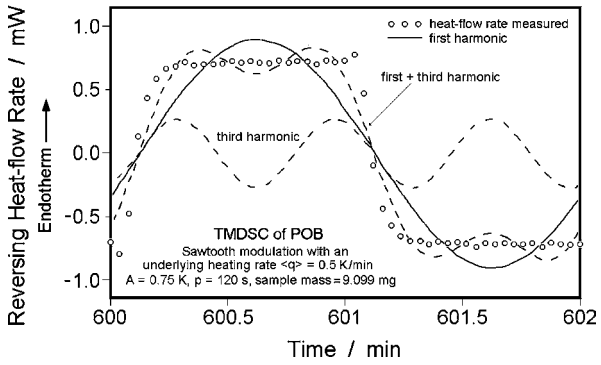

Fig. 2. Typical heat-flow rate, as deconvoluted from TMDSC results on POB using an underlying heating rate, $\langle q \rangle = 0.5$ K/min (pseudo-isothermal analysis [34]), or measured directly on quasi-isothermal TMDSC ($\langle q \rangle = 0.0$ K/min).

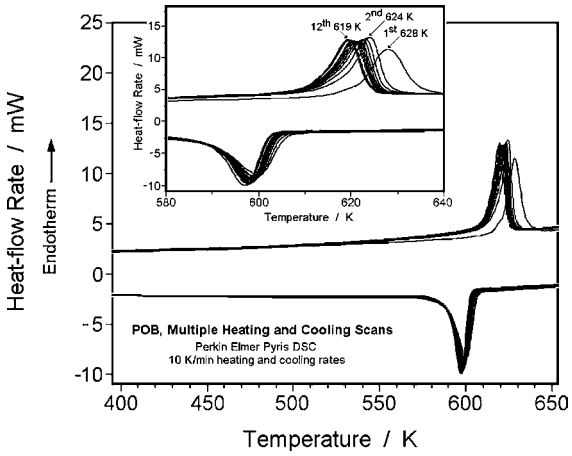

Fig. 3. Standard DSC on repeated heatings followed by coolings of the POB.

For the TMDSC, all calibrations were made at a heating rate of 5 K/min or lower. A typical sawtooth procedure involves heating at 2.0 K/min for 60 s, followed by cooling at 1.0 K/min for another 60 s, so that the period is 120 s and the underlying heating rate, $\langle q \rangle$, is 0.5 K/min with a temperature amplitude about the axis of symmetry of 0.75 K. Up to 600 K the sliding average of the heat-flow rate was changing linearly, i.e., the signal is stationary, which permits deconvolution of the modulated heat-flow rate signal by subtracting the total heat-flow rate from the measured heat-flow rate to yield a pseudo-isothermal analysis [34]. As long as the heat-flow rate response is linear relative to the temperature change, the reversing C_p can be calculated from the first harmonic of the Fourier transformation, as indicated in Fig. 2 on a typical example. The symmetric sawtooth modulation shows only odd harmonics and all higher harmonics have a fixed ratio to the first harmonic as long as the C_p is independent of frequency, and the first harmonic results in the best averaging over the noise. The sum of the first and third harmonic illustrates the increasing approach to the measured data when including higher harmonics. Summing from the first to the ninth harmonic reproduces the experimental data within the uncertainty of measurement. The Pyris version 7.0 software with its heat-capacity-calculation function was used to compute the reversing and total heat capacities directly from the ratio of the first harmonic of the reversing heat-flow rate as a response to the reversing heating rate. Starting at ≈600 K, sufficient latent heats are involved in modulating the sample temperature to make this simple measurement of the reversing C_p nonlinear and nonstationary so that quasi-isothermal experiments with $\langle q \rangle = 0$ have to be performed after waiting until irreversible processes such as annealing and recrystallization have stopped [33,34].

The glass-transition temperatures, T_g, were taken, as usual, at the temperature of half-devitrification of the sample at the given heating rate, as indicated by the increase of the C_p. The samples were cooled before analysis at a similar rate to minimize the enthalpy relaxation (hysteresis). The width, ΔT, of the glass transition region was estimated from the intersection of a tangent at the point of inflection of C_p. For amorphous homopolymers and random copolymers, this width of ΔT is usually between 5 and 10 K, but for the partially ordered copolymers this range increases to as much as 200 K [8,9]. The endothermic transition peaks are sufficiently broad to identify the peak temperatures as the most common species undergoing the transition. The integral of the heat-flow rate over time is taken as the latent heat with an appropriate baseline computed from the C_p [32].

3. Results and data discussion

3.1. Poly(1,4-oxybenzoate)

3.1.1. Stability of the POB sample

To check on the stability of the POB samples to be analyzed, repeating heating and cooling experiments were performed between 383 and 653 K, as shown in Fig. 3. The first heating yields a high T_1 of 628 K and a lower C_p above 550 K, but also, seemingly, a somewhat lower heat of transition. The approximate crystallinities based on the area above a tangential baseline are 64.6, 75.2, and 74.5% for the 1st, 2nd, and 12th heating, respectively (see Section 3.1.2 for a more precise determination of the heat of transition from an analysis with Eq. (1)). The peak temperature decreases to 619 K for the 12th heating cycle and the crystallization temperature decreases as well. The heat capacities below the transition peak after the first heating are reproducible. On continuation of the experiment, the sample changes little, the melting point decreased to 616 K on the 60th cycle. Thermogravimetry showed in the first heating a weight loss of 6.1% below 450 K without a corresponding endothermic peak in the DSC and a further loss of 2.1% between 500 and 700 K. The causes for these initial changes are not fully clear. To avoid the uncertainty caused by the weight loss during the first cycle, only subsequent cycles were used in the analyses. The weight loss in the second heating–cooling cycle in the temperature range of 300–653 K is only 1.7 wt.%. The total mass loss to the 12th heating–cooling cycles is 2.3 wt.%. Further cycles show less than 0.1 wt.% mass-loss per run.

3.1.2. Disordering transition of POB

Fig. 4 illustrates quantitative thermal analysis of POB for a second heating cycle. Fig. 4a illustrates the experimental, apparent, molar $C_p^{\#}(\mathrm{exp})$ from 450 to 650 K. The sharp transition at 623.7 K corresponds to the orthorhombic crystal-to-condis-crystal transition seen in the phase diagram of Fig. 1. Above T_g of all non-crystalline fractions, the fractional crystallinity can be calculated by a two-phase model [35]:

$$C_p^{\#}(\mathrm{exp}) = w_c C_p(\mathrm{solid}) + (1 - w_c) C_p(\mathrm{liquid}) - \left(\frac{\mathrm{d}w_c}{\mathrm{d}T}\right) \Delta H_d(T), \quad (1)$$

where $(\mathrm{d}w_c/\mathrm{d}T)\,\Delta H_d(T)$ is the latent heat exchanged per kelvin of increase in temperature. The $C_p(\mathrm{solid})$ and $C_p(\mathrm{liquid})$ are the calculated crystalline and melt heat capacities as a function of temperature [9,32], and $\Delta H_d(T)$ is also known from the dependence of these heat capacities on temperature $[\mathrm{d}\Delta H_d/\mathrm{d}T = C_p(\mathrm{liquid}) - C_p(\mathrm{solid})]$. The value of $C_p(\mathrm{liquid})$ is derived from the easily measured

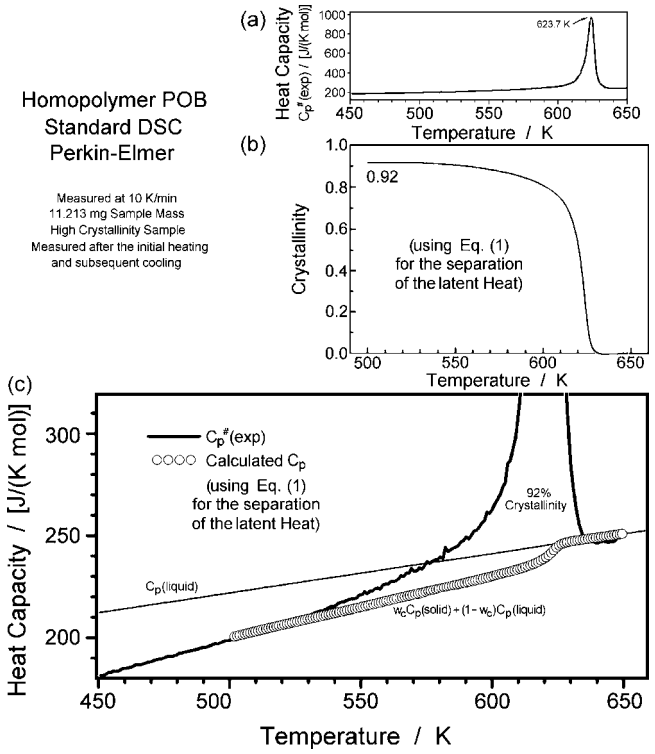

Fig. 4. Standard DSC of POB, analyzed with the advanced thermal analysis system (ATHAS) [32]: (a) apparent experimental heat capacity; (b) calculated crystallinity using the data [8,9] and the two-phase model of Eq. (1); (c) the three heat capacity terms of Eq. (1): $C_p^{\#}(\text{exp})$, $C_p(\text{liquid})$, and $w_c C_p(\text{solid}) + (1 - w_c)C_p(\text{liquid})$.

anisotropic melts of the copolymers which are strictly additive. Its values are also available from the advanced thermal analysis system (ATHAS) data bank [8]. The $C_p(\text{solid})$ is calculated from the vibrational spectrum fitted to the low-temperature C_p, as determined in Ref. [9]. Fig. 4b shows the fractional crystallinity for the analyzed POB. At low temperature, the crystallinity reaches a maximum value of 92 wt.%. The crystallinity function, $w_c = f(T)$ of Fig. 4b was then used to calculate C_p. The result is given by the open circles in Fig. 4c. Above 500 K, the measured C_p increases gradually above the calculated values, indicating the absorption of latent heat.

The approximate crystallinities reported in Fig. 3 for the various heating and cooling experiments are lower than calculated with Eq. (1) by as much as 20% since in Fig. 3 the change of C_p with temperature could not be considered and a simple, linear baseline was chosen. The lower C_p on first heating seen in Fig. 3 may indicate that the initial sample is close to 100% crystalline. The disordering peak, broadened towards higher temperature may indicate superheating, indicative of more perfect crystals, but such may also be observed for as-polymerized, high-molar-mass samples. The data were not sufficiently reproducible and uniform from sample to sample for a more quantitative analysis as done with Fig. 4.

A measurement of $C_p^{\#}(\text{exp})$ on third heating is shown in Fig. 5. From 365 to 410 K $C_p^{\#}(\text{exp})$ is in good agreement with the calculated C_p of the solid [9]. The relative deviation from the earlier data is less than 2%. The $C_p^{\#}(\text{exp})$ measured by standard DSC does not show a sharp glass transition, but reaches the level of the liquid (anisotropic melt) at the end of the disordering transition [8]. Because of the closely similar molecular motions in the melt and in an unisotropic melt, their heat capacities are practically identical as long as the small degree of order in the unisotropic melt does not change with temperature. The presence of a broad glass transition or the existence of a rigid-amorphous

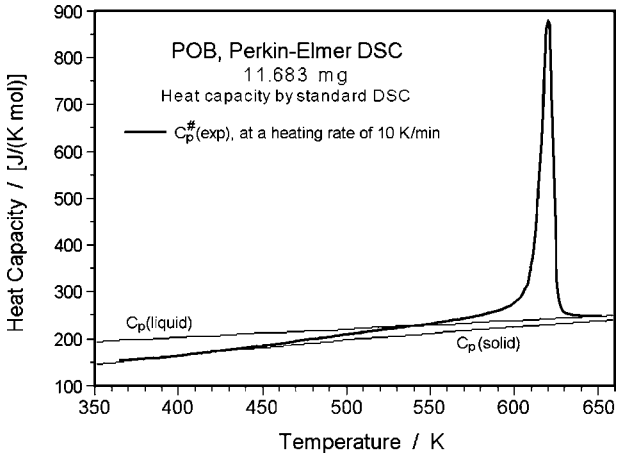

Fig. 5. Standard DSC of POB, expressed as $C_p^{\#}(\text{exp})$. Data from a third heating cycle (see Fig. 3). The thin lines represent the liquid and solid data of Ref. [8,9].

fraction (RAF) cannot be clearly identified without measurements by temperature-modulated calorimetry, as will be shown next.

3.1.3. Temperature-modulated calorimetry

The reversing C_p from the temperature modulation with an underlying heating rate is shown in Fig. 6 as the dashed line (note the expanded scale relative to Fig. 5). Compared to the $C_p^{\#}(\text{exp})$ by standard DSC, indicated by the solid line, the reversing C_p shows lower values above ca. 480 K. One concludes that up to this temperature the measured, apparent $C_p^{\#}(\text{exp})$ is practically reversible. The time-dependence of the heat capacity due to the glass transition is not sufficient to show up in the reversing C_p. The glass transition seems to occur between about 410 and 480 K, a rather broad range which may include in the higher temperatures the devitrification of a RAF. In the melting range, the reversing C_p shows a peak temperature at 617.8 K which is slightly less than the standard DSC peak temperature of Fig. 3, with 620.3 K. This increase may simply arise from the larger instrument lag of the standard DSC at 10 K/min. The total C_p of the TMDSC has a similar peak temperature (617.6 K), but with a somewhat larger peak height than the standard DSC, again, indicating the temperature lag and in addition a loss of stationarity due to the latent heat [33].

The quasi-isothermal data in Fig. 6 are given by the open circles. They represent measurements during the last 10 min of the 30 min experiments. Up to about 585 K, these heat capacities are identical to the measurement with an underlying heating rate (dashed

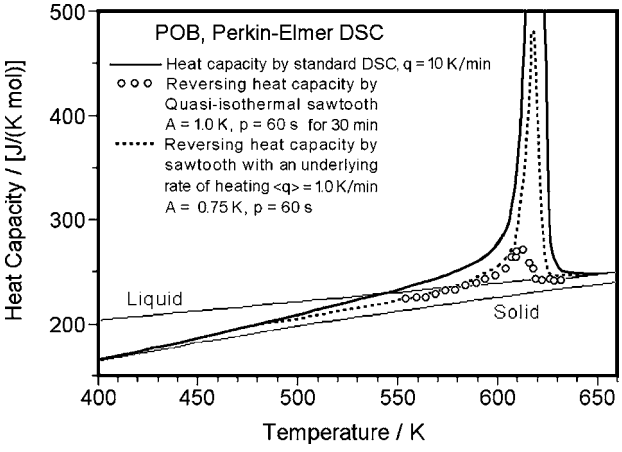

Fig. 6. Comparison of DSC, TMDSC, and quasi-isothermal TMDSC of POB.

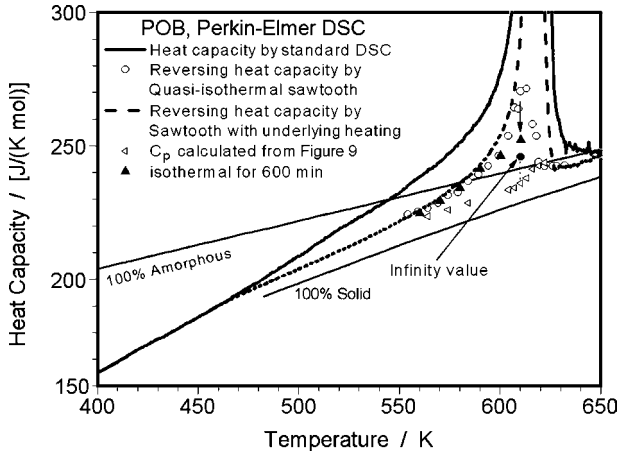

Fig. 7. Time-dependence of the reversing heat capacity of POB.

line), and at higher temperature they show a much-reduced peak. At the given frequency, the reversing C_p is close to reversible up to 585 K, and above, the reversing C_p contains increasing contributions from latent heats with longer relaxation times than can decay at the underlying heating rate.

To find the upper temperature limit of reversibility, a time-dependent, quantitative analysis was carried out, as given in Fig. 7. Note the further expanded scale of C_p relative to Fig. 6. Additional quasi-isothermal data were measured with an expanded modulation period to 600 min. These points are marked by the filled triangles. These longer modulation times extend the temperature region of (slow) reversible response to 600 K. Finally, the kinetics of the change in C_p with time from 560 to 610 K was measured and is illustrated in Fig. 8. The residual crystallinity at the end of the 600 min experiments was measured by standard DSC, as shown in Figs. 9 and 10, finally, displays the details of the analysis of the data at 610 K, including the extrapolation to infinite time, using the indicated double-exponential function. This extrapolation should give an estimate of the reversible C_p at 610 K. It is entered into Fig. 7 as the filled circle.

For the whole temperature range from 470 K to the end of the disordering transition one can see a remaining slow increase in the reversible C_p. It is much less than that of the reversing C_p, but ultimately exceeds C_p(liquid) by a small mount. This may well be due to an increase in mobility (disorder) within the crystals, as was

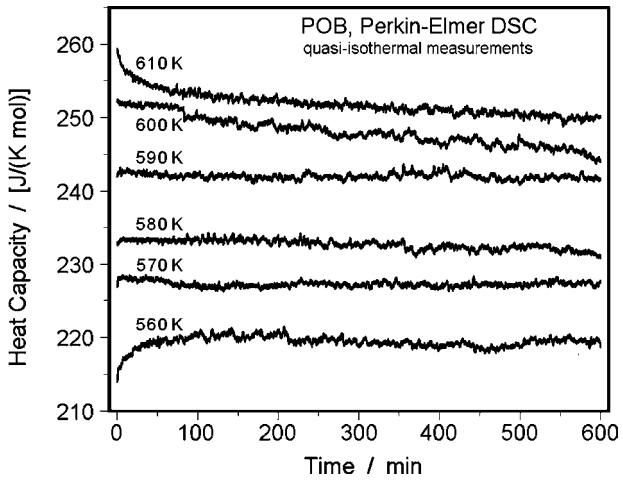

Fig. 8. Change of the heat capacity of POB with time (selected data points are also seen plotted in Fig. 7).

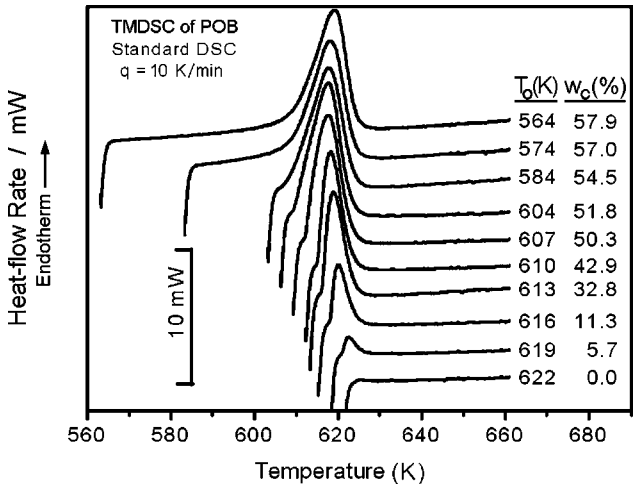

Fig. 9. Estimation of the crystallinity of POB after 600 min of modulation by standard DSC. Note that at lower temperatures these estimated crystallinities may have to be increased by up to +15% (compare to the graph of crystallinity drawn in Fig. 4).

observed earlier in the polyoxides [36] and nylons [37]. In these cases a true glass transition of the crystal was reached (without change in crystal structure). If some of this increase in reversible heat capacity were due to locally reversible melting, as observed for most chain-folded, semicrystaline polymers, it would be much less than commonly seen [33]. The more rigid polymers, such as poly(oxy-2,6-dimethyl-1,4-phenylene), has no locally reversible melting [33], in accord with the small or no reversible melting in POB. For flexible, linear macromolecules the reversible, local latent heat was also observed to decrease for more perfect crystals and go to zero for extended-chain polymers and for once and twice-folded crystals of high perfection [36,38].

3.2. Poly(2,6-oxynaphthoate)

The analysis of PON is illustrated with Fig. 11. The standard DSC curve after cooling from the anisotropic melt shows a sharp disordering transition at 670 K which has a broad cold-crystallization or reorganization minimum starting at ≈540 K, accounting for much of the endotherm seen on disordering. From 320 K the C_p by standard DSC and continuing from 420 to 560 K the reversing C_p and

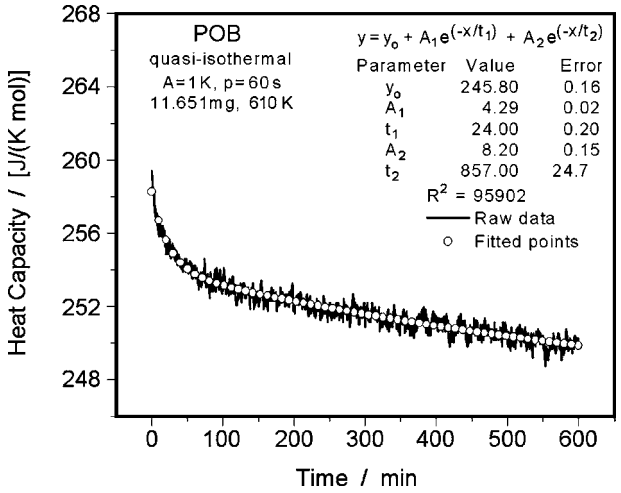

Fig. 10. Evaluation of the decrease in reversing melting at 610 K with a plot of the apparent reversing C_p. The equation given in the figure permits the extrapolation to infinite time.

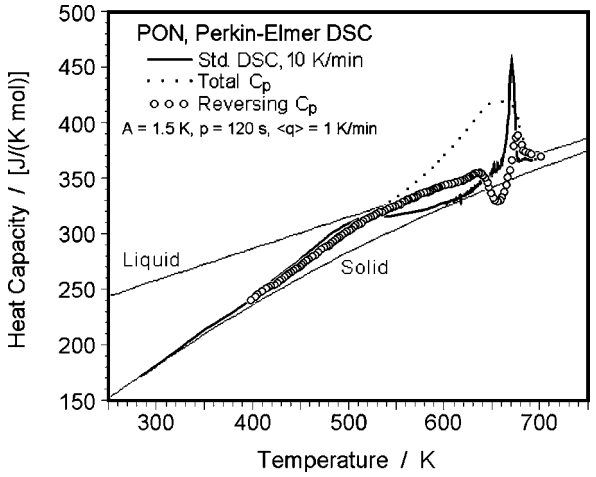

Fig. 11. Standard DSC and TMDSC of PON (TMDSC from sawtooth modulations, run with an underlying heating rate of 1 K/min).

TMDSC change from the C_p of the solid to that of the liquid, suggesting a very broad glass transition. This broad transition may involve the amorphous, rigid-amorphous, and ordered phases, with the overall T_g being shifted by a small amount of ordering to about 460 K, 40 K higher than the T_g shown in the phase diagram of Fig. 1. The surprising difference between the total C_p by TMDSC and DSC is a measure of the different behavior of the two samples on slow and fast heating. Because of the small heat-flow rate up to ≈610 K, one expects full linearity and stationarity of the calorimeter response. Under such conditions, the larger total endotherm by TMDSC is due to a ordering and disordering, so that the integral of C_p(total) over T shows an endotherm of several times the size measured by standard DSC [32]. Overall, the dynamics of this disordering and ordering is irreversible.

3.3. The copolymers

All copolymers were hot pressed at about 550 K to make films with thickness of 1.0 mm to achieve good contact within the calorimeter pan. As with the homopolymers, the copolymers were measured after establishing a thermal history by cooling from the anisotropic melt with a cooling rate of 10 K/min.

The DSC curves of P(HBA-*co*-HNA) of different composition are summarized in Fig. 12. For the 30/70 copolymer cooling after heating shows a supercooling of ≈58 K before crystallization, similar to other aromatic copolyesters [33]. The C_p of the copolymer on heating is shown in Fig. 12a. A T_g is shown between 360 and 390 K, but may continue on to higher temperature, perhaps as unfreezing of a rigid-amorphous fraction. The C_p curve from the standard DSC shows a relatively sharp disordering transition at ≈590 K. The reversing C_p from the sawtooth modulation with underlying heating shows an almost totally irreversible latent heat at the disordering transition and suggests that most or all of the increase in

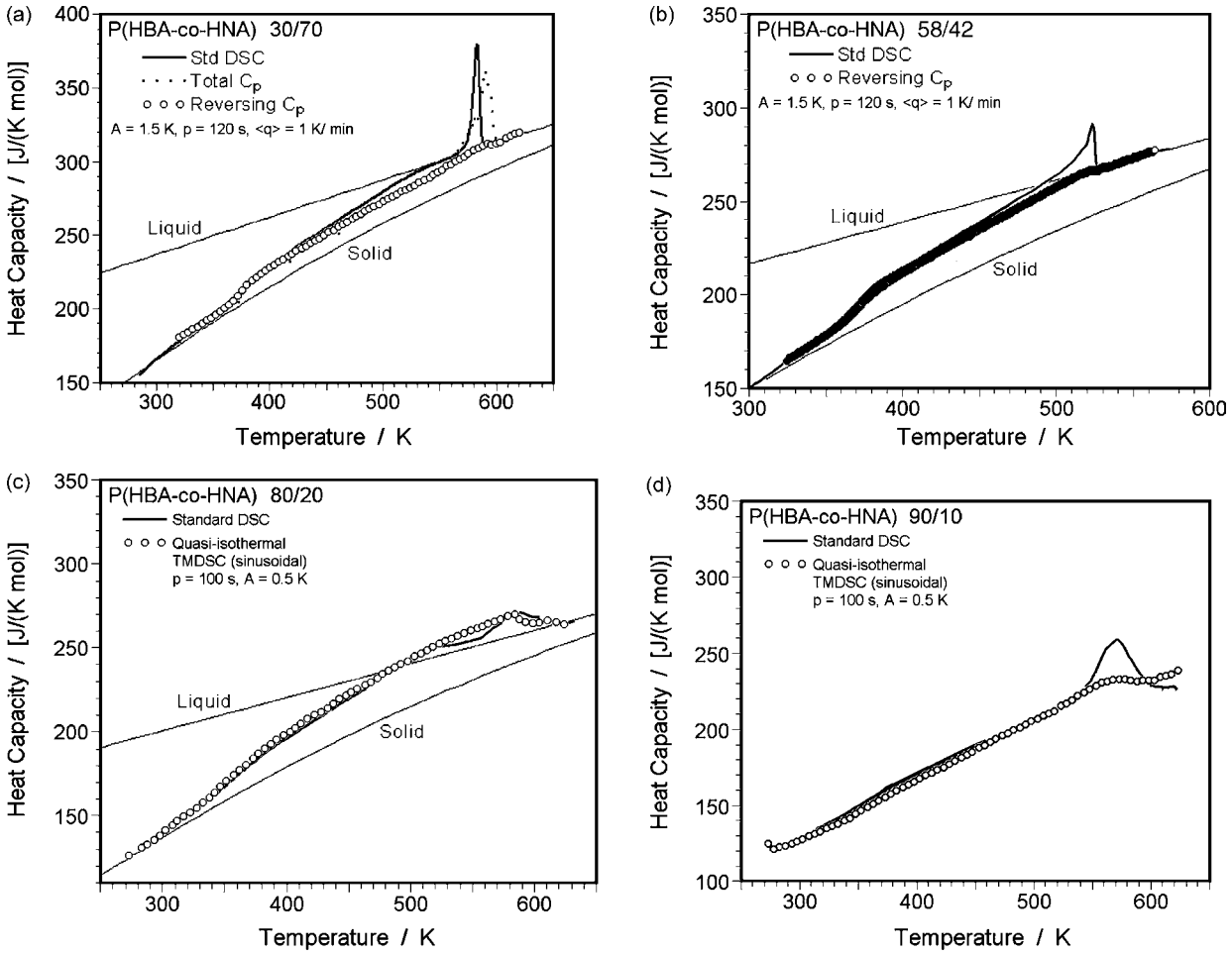

Fig. 12. Standard DSC and TMDSC of the copolymers: (a) P(HBA-*co*-HNA) 30/70; (b) P(HBA-*co*-HNA) 58/42; (c) P(HBA-*co*-HNA) 80/20; (d) P(HBA-*co*-HNA) 90/10 (the TMDSC in (a) and (b) are from sawtooth modulations run with an underlying heating rate and in (c) and (d) from quasi-isothermal measurements with sinusoidal modulation).

reversing heat capacity is reversible and is more likely due to a glass transition of the RAF and the crystals than local reversible melting.

The standard DSC curve of P(HBA-*co*-HNA) 58/42 in Fig. 12b shows a single endotherm. On cooling, the initial crystallization peak is even sharper than the melting peak and a supercooling of ≈42 K is observed. The reversing C_p of the copolyester in Fig. 12b illustrates a T_g in the temperature range from 350 to 385 K, again followed, perhaps, by a broad softening range of a rigid amorphous fraction. The reversing C_p by TMDSC with sawtooth modulation using an underlying heating rate shows an almost totally irreversible transition as was also seen in Fig. 12a.

For the 80/20 copolymer, two shallow endothermic peaks were found by standard DSC at 519 and 583 K, corresponding to the rigid-to-condis-crystal transition (T_1) and the condis-to-condis-crystal transitions (T_3) shown in the phase diagram of Fig. 1. After eliminating much of the thermal history and fitting to the C_p of the solid, the apparent heat capacities are shown in Fig. 12c. The cooling curves by standard DSC show one sharp and one broad exotherm, corresponding to the two thermal transitions, indicating considerable supercooling. The T_g is shown in the range of ca. 300–400 K. The quasi-isothermal results show, again, the possibility of a subsequent glass transition of a rigid-amorphous fraction overlapping with the rigid-to-condis-crystal transition.

Finally, Fig. 12d shows the thermal analysis for the 90/10 copolyester. The endotherm on heating occurs at ≈570 K, the exotherm on cooling at ≈545 K, indicating considerable supercooling of the crystals. In accord with this observation by standard DSC, the reversing C_p during this transition indicates only little reversing melting. Both the C_p from standard DSC and reversing C_p from the quasi-isothermal TMDSC show the T_g from 330 to 380 K.

As the HNA content decreases, the semicrystalline structure of the copolymers change from the single disordering peak prior to their thermal decomposition seen for PON to the double peak in POB. The absence of this polymorphism of these copolymers with larger HNA concentration is probably due to the increased randomness caused by the HNA relative to the HBA. The remaining crystallinity found for all copolymers is probably due to a partial isomorphism of the HBA and HNA monomer precursors, as proposed by Biswas and Blackwell [19–21] and is also observed, for example, in the copolymer systems poly(ethylene terephthalate-*co*-isophthalate) [33].

4. Conclusions

The behavior of all samples was discussed on hand of the phase diagram of Fig. 1 [14]. Of the samples analyzed, only the POB homopolymer had a high crystallinity (see Fig. 4). Outside the transition ranges, the solid and liquid heat capacities derived from TMDSC were in agreement with the prior derived DSC data [8,9], also available in the ATHAS data bank and show additivity for the copolymers [8]. All transitions are largely irreversible (see Figs. 7, 11 and 12). In the melting-peak area the reversing C_p is frequency dependent. Above the glass transition, the reversible C_p increases above that calculated from the crystallinity, probably due to an increase of mobility within the crystals and/or a possible rigid-amorphous fraction (mainly in the copolymers). Additional high-precision X-ray diffraction on well-characterized samples is necessary to resolve the effect on crystal and amorphous fractions. For the homopolymers, as well as copolymers, there is little or no local, reversible melting seen, in contrast to the more flexible linear macromolecules [33]. This low fraction of reversible melting agrees with the absence in reversible melting in the similarly rigid and high-melting poly(oxy-2,6-dimethyl-1,4-phenylene) [33].

Acknowledgments

This work was supported by the Division of Materials Research, National Science Foundation, Polymers Program, Grant #DMR-0312233. Use of some of equipment and laboratory space was provided by the Division of Materials Sciences and Engineering, Office of Basic Energy Sciences, U.S. Department of Energy at Oak Ridge National Laboratory, managed and operated by UT-Battelle, LLC, for the U.S. Department of Energy, under contract number DOE-AC05-00OR22725.

References

[1] G.W. Calundann, M. Jaffe, Proc. Robert A. Welch Found. Conf. Chem. Res. 26 (1982) 247.
[2] G.H. Ba, E.F. Cluff, in: A. Blumstein (Ed.), Polymeric Liquid Crystals, Plenum, New York, 1985, p. 217.
[3] M.G. Dobb, J.E. McIntyre, Adv. Polym. Sci. 60–61 (1984) 61.
[4] J.B. Stamatoff, Mol. Cryst. Liq. Cryst. 110 (1984) 75.
[5] J. Blackwell, A. Biswas, in: I.M. Ward (Ed.), Developments in Oriented Polymers-2, Elsevier, Barking UK, 1987 (Chapter 5).
[6] G.D. Butzbach, J.H. Wendorff, H.J. Zimmerman, Makromol. Chem. Rapid Commun. 6 (1985) 821.
[7] G.D. Butzbach, J.H. Wendorff, H.J. Zimmerman, Polymer 27 (1986) 1337.
[8] M.Y. Cao, B. Wunderlich, J. Polym. Sci. Polym. Phys. Ed. 23 (1985) 521; see also the experimental data of the updated ATHAS Data Bank: M. Varma-Nair, B. Wunderlich, J. Phys. Chem., Ref. Data 20 (1991) 349.
[9] M.Y. Cao, M. Varma-Nair, B. Wunderlich, Polym. Adv. Technol. 1 (1990) 151.
[10] S.Z.D. Cheng, Macromolecules 21 (1988) 2475.
[11] D.Y. Yoon, N. Masciocchi, L.E. Depero, C. Viney, W. Parrish, Macromolecules 23 (1990) 1793.
[12] J. Economy, W. Volksen, C. Viney, R. Geiss, R. Siemens, T. Karis, Macromolecules 21 (1988) 2777.
[13] A. Mühlebach, J. Lyerla, J. Economy, Macromolecules 22 (1989) 3741.
[14] A. Habenschuss, M. Varma-Nair, Y.-K. Kwon, J. Ma, B. Wunderlich, Polymer 47 (2006) 2369.
[15] B. Wunderlich, M. Möller, J. Grebowicz, H. Baur, Adv. Polym. Sci. 87 (1988) 1.
[16] H.R. Kricheldorf, G. Schwarz, Polymer 31 (1991) 481.
[17] G. Schwarz, H.R. Kricheldorf, Macromolecules 24 (1991) 2829.
[18] S.Z.D. Cheng, J.J. Janimak, A. Zhang, Z. Zhou, Macromolecules 22 (1989) 4240.
[19] A. Biswas, J. Blackwell, Macromolecules 21 (1988) 3146.
[20] A. Biswas, J. Blackwell, Macromolecules 21 (1988) 3152.
[21] A. Biswas, J. Blackwell, Macromolecules 21 (1988) 3158.
[22] S. Hanna, T. Lemmon, R.J. Spontak, A.H. Windle, Polymer 33 (1992) 3.
[23] A.H. Windle, C. Viney, R. Golombok, A.M. Donald, G.R. Mitchell, Trans. Farad. Soc. 79 (1985) 55.
[24] S. Hanna, A.H. Windle, Polymer 29 (1988) 207.
[25] B. Wunderlich, J. Chem. Phys. 29 (1958) 1395.
[26] H.C. Langelaan, A. Posthuma de Boer, Polymer 37 (1996) 5667.
[27] D.S. Kalika, D.Y. Yoon, Macromolecules 24 (1991) 3404.
[28] H. Bechtholdt, J.H. Wendorff, H.J. Zimmermann, Macromol. Chem. 188 (1987) 651.
[29] G.W. Calundann, US Patent (1970) 4,161,470.
[30] H.R. Kricheldorf, G. Schwarz, F. Ruhser, Macromolecules 24 (1991) 3485.
[31] H.R. Kricheldorf, F. Ruhser, G. Schwarz, Macromol. Chem. Phys. 192 (1991) 2371.
[32] B. Wunderlich, Thermal Analysis of Polymeric Materials, Springer, Berlin, 2005.
[33] B. Wunderlich, Prog. Polym. Sci. 28 (2003) 383.
[34] B. Wunderlich, Y. Jin, A. Boller, Thermochim. Acta 238 (1994) 277.
[35] S.F. Lau, H. Suzuki, B. Wunderlich, J. Polym. Sci. Polym. Phys. 22 (1984) 379.
[36] W. Qiu, M. Pyda, E. Nowak-Pyda, A. Habenschuss, B. Wunderlich, Macromolecules 38 (2005) 8454.
[37] W. Qiu, A. Habenschuss, B. Wunderlich, Polymer 48 (2007) 1641.
[38] W. Qiu, M. Pyda, E. Nowak-Pyda, A. Habenschuss, Wunderlich, J. Polym. Sci. B: Polym. Phys. 45 (2007) 475.